Journal of Applied Polymer Science

Polyaniline benefited from poly(vinyl alcohol) in both conductivity and energy storage

Liuqing Yang,[1,2] Wenling Wu,[2] Yang Feng,[1] Yingxia Ma,[2] Shengtao Li,[1] Yanfeng Li[2]

[1]State Key Laboratory of Electrical Insulation and Power Equipment, School of Electrical Engineering, Xi'an Jiaotong University, Xi'an 710049, People's Republic of China

[2]State Key Laboratory of Applied Organic Chemistry, College of Chemistry and Chemical Engineering, Lanzhou University, Lanzhou 730000, People's Republic of China

Correspondence to: S. Li (E-mail: sli@mail.xjtu.edu.cn)

ABSTRACT: Polyaniline (PANI) is an important conductive polymer because of its wide potential. In this article, we present a modified chemical polymerization method, which employs poly(vinyl alcohol) (PVA) as a doping assistant, for the synthesis of PANI. In this study, the introduced PVA contributed both to the conductivity and specific capacitance. The conductivity markedly increased more than two orders of magnitude from 5.2 to 1052 S/m after a small amount of PVA was introduced. A combination of the amphoteric polymer and acid together as the dopant extended the doping method for the synthesis of conductive PANI. The specific capacitance of PANI occurred up to 382.9 F/g at a current density of 0.5 A/g. The PANIs exhibited fast redox reactions, good ion response, and a short diffusion path of electronic transport. By feat of the hydrophilicity of PVA, the as-prepared PANI showed a good dispersibility in aqueous solution; this is important for its potential applications. © 2015 Wiley Periodicals, Inc. J. Appl. Polym. Sci. **2016**, *133*, 42989.

KEYWORDS: composites; conducting polymers; electrochemistry; properties and characterization; surfactants

Received 12 June 2015; accepted 25 September 2015

DOI: 10.1002/app.42989

INTRODUCTION

Polyaniline (PANI) has captured much attention during past decades because of its wide potential applications; these include applications in energy storage,[1–5] sensors,[6–8] smart devices,[9–12] electronic static discharge,[13,14] electromagnetic interference shielding,[15–20] and anticorrosion coatings.[21] Its potential applications depend on its relatively facile synthesis,[22–24] low cost,[25] and easily varied physicochemical properties.[26–29] However, the potential applications of PANI have been limited by its poor conductivity and processability.[30]

PANI is unique among conducting polymers because of its simple acid/base doping/dedoping chemistry and further reversible control of electrical properties.[31–33] The degrees of doping and oxidation levels are two crucial factors that affect its electrical conductivity. Half-oxidized PANI with about 50% doping is expected to exhibit the highest conductivity in theory. In addition to the degrees of doping and oxidation levels, the conductivity of PANI also strongly depends on the type of dopant.[34,35] On the basis of this observation, the reported conductivity of PANI in the acid form varies from approximately 1 to 100 S/cm. However, it is regretful that almost the entire effort to improve the conductivity of PANI has been focused on various one-component polymeric sulfonic-type proton dopants,[36–41] and little emphasis[42] has been placed on other possible dopants; this raises a question that unwittingly opens the door to lots of potential impurities in the achievement of the alleged optimal 50% doping level.[43,44]

In addition, the improvement of the processability of PANI is still an important research aspect for PANI. As is common with other conjugated polymers, PANI is poorly thermally processable and almost insoluble in most common solvents. On the basis of this, dozens of synthesis methods[14,17,42,45–55] have been developed to synthesize dispersible and solvable PANI; these include the template method, self-assembly, blending, *in situ* polymerization, grafting, and electrochemical and interfacial polymerization. Dispersed PANI in different solvents with regular kinds of morphology is subsequently obtained. The dispersion homogeneity is an important factor for making composites with uniform properties. In this way, one may achieve the desired properties for each application by varying the polymer

Additional Supporting Information may be found in the online version of this article.

matrix. However, simple ways for preparing well-dispersible PANI are still a scientific challenge.

In this study, we introduced poly(vinyl alcohol) (PVA) as a doping assistant into a typical PANI polymerization process and chose sulfuric acid (H_2SO_4) as the proton provider for comparison purposes. Obviously, the additive PVA, together with H_2SO_4, played an active role in promoting the conductivity of PANI to some extent and put the PANI in the range of good semiconductors. The as-prepared PANI was very dispersible in aqueous solution and bypassed the scientific challenge of difficult processing. The properties of the PANI composite as the supercapacitor electrode materials were also investigated.

EXPERIMENTAL

Synthesis of PANI in the Presence of PVA (PANI/PVA)

Aniline (ANI) monomer (analytical reagent) was distilled under reduced pressure. Ammonium persulfate (analytical reagent) and PVA (DP 1700, degree of hydrolysis 88%) were used as received without further treatment. Polytetrafluoroethylene (PTFE) in the form of a 60% aqueous dispersion was purchased from Sigma-Aldrich. All other reagents were commercially available. A facile method was used to prepare PANI/PVA. In a typical process, a desired quality of PVA was added to water (30 mL) with constant gentle stirring at room temperature until it was completely dissolved. Then, ANI (0.93 g, 10 mmol) was added to the previous solution for 1 h, and the resulting solution was cooled to 0°C in a mixed ice–water bath. H_2SO_4 (1 mol/L) was dropped into the solution slowly over 1 h, and then, ammonium persulfate (2.28 g, 10 mmol) dissolved in water (10 mL) was dropped in slowly. The reaction system was preserved at a constant temperature of 0°C and a constant stirring rate for 24 h. The resulting product was collected by centrifugation, washed with ethanol and deionized water, and finally, dried at 60°C in a vacuum oven. To prepare a parallel sample, PANI without PVA was synthesized according to the previous method.

Instrumentation

Fourier transform infrared (FTIR) spectra were recorded on a Nicolet Magna-IR 550 spectrophotometer in the range 4000–400 cm^{-1} with the KBr pellet technique. X-ray diffraction (XRD) patterns were recorded with nickel-filtered Cu Kα radiation ($\lambda = 0.154$ nm) with a Rigaku D/MAX 2400 diffractometer. X-ray photoelectron spectroscopy (XPS) analysis was performed on a Thermon Scientific K-Alpha surface analysis with X-ray monochromatization. Electronic conductivity was measured on a compacted circle slice by standard four-probe resistance with a Jingge Electronic ST 2253 measurement system. Ultraviolet–visible (UV–vis) absorption spectra were recorded from 270 to 1100 nm with a Persee TU-1810 UV–vis spectrophotometer in a quartz cuvette.

The sample, which possessed the highest conductivity, used for FTIR and XPS testing was prepared at a PVA/ANI ratio of 0.063 w/w. The PANI/PVA samples (1 mg) were sonicated in deionized water (10 mL) for 24 h; then, the liquid supernatant was used for UV–vis characterization and photos.

Electrochemical Measurement

The electrode performance was measured by a three-electrode configuration in a beaker-type electrochemical cell equipped with a working electrode, platinum as the counter electrode, and a saturated calomel electrode (SCE) as the reference electrode.

Two kinds of working electrodes were used in experiments. One of them was an active-material-modified glassy carbon electrode with a diameter of 3 mm; typically, the samples (1 mg) were ultrasonically dispersed in deionized water (1 mL), and the PTFE emulsion (60%, 10 μL) was added to the dispersion. The previous suspension (5 μL) gun was dropped onto the glassy carbon electrode with a pipet and dried at room temperature. This electrode, a platinum wire as a counter electrode, was then used for the determination of the cyclic voltammetry (CV) and electrochemical impedance spectroscopy because it had a higher sensitivity.

The other sample was prepared by the mixture of active material (80 wt %), acetylene black (7.5 wt %), graphite (7.5 wt %), and a PTFE emulsion (5 wt %). The slurry was spread onto a square stainless steel mesh with a 1-cm^2 geometry area. The electrode was heated at 60°C for 24 h to evaporate the solvent. This electrode, a platinum sheet as a counter electrode, was then used for the determination of the galvanostatic charge–discharge because it was closer to the real capacitor.

The electrolyte was a 1*M* H_2SO_4 aqueous solution. The CVs, galvanostatic charge–discharge, and electrochemical impedance spectroscopy were measured by a CHI 660B electrochemical workstation. The CV experiments were performed within the potential range of −0.2 to 0.8 V (vs SCE) at scan rates from 5 to 100 mV/s. Galvanostatic charge–discharge was carried out at current densities of 0.5, 1, and 2 A/g, respectively. The electrochemical impedance spectroscopy was recorded under the following conditions: alternating-current voltage amplitude = 5 mV and frequency range = 0.1–10^5 Hz at 0.4 V.

RESULTS AND DISCUSSION

Structure of PANI/PVA

The structure of PANI/PVA (PVA/ANI 0.063 w/w) was characterized by FTIR spectroscopy. Figure 1(a) shows the typical FTIR spectra of PANIs synthesized in the absence and presence of PVA 1788. It was obvious that both curves presented the characteristic absorption peaks of PANI. The single peaks around 3435 cm^{-1} represented N—H and O—H stretching vibrations. The peak intensity decreased dramatically in the composite; this reflected the existence of hydrogen bonding between the PANI amine groups and the oxygen in the PVA chains. Such an interaction indicated that the PANI/PVA blend was miscible.[56] The peaks around 3229 cm^{-1} were the Fermi resonance between the frequency doubling of —NH_2 bending vibrations and —NH_2 stretching vibrations. The peaks at 1620 cm^{-1} were attributed to —NH_2 bending vibrations. The characteristic absorbances at about 1562 and 1477 cm^{-1}, due to the symmetrical paradisubstituted skeletal vibrations of the quinoid ring and benzene ring, respectively, demonstrated that the PANI was prepared and existed in the emeraldine form. The ratio of the area under these two peaks was proportional to the ratio of quinoid to benzenoid structures. The peaks around 1301 cm^{-1}

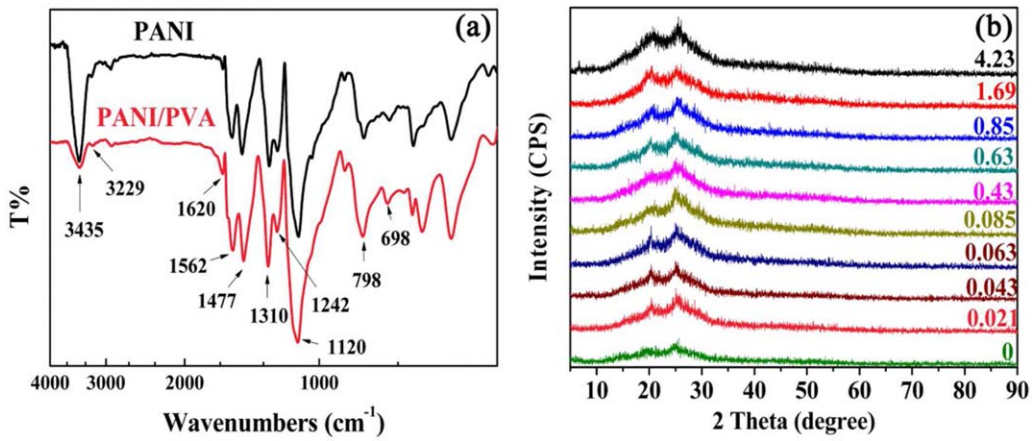

Figure 1. (a) FTIR spectra of PANI and PANI/PVA at a PVA/ANI ratio of 0.063 w/w. (b) XRD patterns of PANI at different PVA/ANI ratios w/w. [Color figure can be viewed in the online issue, which is available at wileyonlinelibrary.com.]

represented typical C—N stretching vibrations in aromatic amine. The C—H bending bands of the benzenoid ring and quinoid ring appeared in the regions 1275–1000 cm^{-1} (in-plane bending) and 900–690 cm^{-1} (out-of-plane bending). Therefore, the results of FTIR spectroscopy demonstrates that the PANI was prepared and existed in the conducting emeraldine form.

Figure 1(b) shows the XRD patterns of the PANI composites synthesized under different conditions. Two broad peaks centered at 2θ values of 20.5 and 25.0–25.5° were observed in the XRD pattern; these are common to amorphous powder and revealed that the nature of the PANI composite was amorphous. The peak centered at a 2θ value of 20.5° (4.33 Å) was ascribed to the periodicity in the direction parallel to the polymer chain, whereas the peak at a 2θ value of 25.0–25.5° (3.56–3.49 Å) was due to the periodicity in the direction perpendicular to the polymer chain.[57] The PVA/ANI ratio almost did not influence the crystallinity of PANI.

Figure 2 shows the XPS spectra for PANI/PVA. The N 1s XPS core level spectrum is shown in Figure 2(a). The three peaks with binding energy at 401.85, 400.57, and 399.52 eV were assigned to positively charged nitrogen (N^+), benzenoid amine (—NH—), and quinoid imine (=N—), respectively.[58,59] The doping level, estimated from the N/S atom ratio, was found to be 2.09 for the sample; this was close to the expected doping level (N/S = 2). The C 1s data [Figure 2(b)] also demonstrated the relative amounts of C—C, C—N, C=N, and C—O by the peaks characteristic for these bonding environments. C—O was observed at 286.00 eV, C—N and C=N were observed at 285.10 eV, and the C—C peak appeared at 284.60 eV.[4,59] The O1s signals [Figure 2(c)] were decomposed into two components. The lower energy peaks (531.60 eV) were attributed to the SO_4^{2-} species, and the higher energy peaks (532.95 eV) were attributed to the C—O—C groups in the surfactant. Finally, the sulfur peaks at 169.57 and 168.40 eV, which were assigned to the sulfate ion, were clearly visible [Figure 2(d)].

Dispersibility of PANI/PVA in an Aqueous Solution

Figure 3 shows the digital images of PANI/PVA dispersed in aqueous solution with different PVA/ANI ratios. We noticed that the dispersibility of PANI/PVA in water was heightened along with the increase in the PVA ratio in light of the gradually darkened color. However, when synthesized with the high PVA/ANI ratio, the composite was rigid and hardly porphyrized.

The increasing dispersibility might have been due to the good hydrophilic properties of PVA 1788. As is well known, PVA, a surfactant, a amphipathic and hydrophobic solubilized substance. Hence, when the hydrophobic monomer ANI was added to the aqueous solution containing the surfactant, it entered the hydrophobic cavity formed by the surfactant and formed a large number of hydrogen bonds between them. Combined with the hydrophilic PVA through abundant hydrogen bonds, the ANI monomer was well dispersed in water; after polymerization, the PANI was potentially more hydrophilic. As a result, PANI/PVA showed good dispersion properties in water.

Room-Temperature Conductivity

Demonstrated in Figure 4(a) are the changes in the room-temperature conductivity of PANI synthesized under different PVA/ANI ratios. It was obvious that the additive PVA played an active role in promoting the conductivity of PANI to some extent. In the beginning, the conductivity of PANI rocketed along with the increasing PVA/ANI ratio from 5.2 S/m (PVA/ANI 0 w/w) to 1052 S/m (PVA/ANI 0.063 w/w), a marked promotion of more than two orders of magnitude for no other reason than that a very small amount of PVA was introduced. This put the PANI in the range of good semiconductors. Nevertheless, the addition of PVA was not always positive. The conductivity dropped with further increases in the PVA/ANI ratio beyond a maximum value. It tended to gently decline beyond a ratio of 1.69 w/w and reached a bottom value of 1.37 S/m at a ratio of 4.22 w/w.

The PVA benefit to the conductivity of PANI might have been caused by several factors as follows:

1. First, the PVA chains incorporated with PANI by hydrogen bonding; this resulted in the change of the PANI orbital electron state and also the band gap energy for electronic transition. This was consistent with the results of the UV–

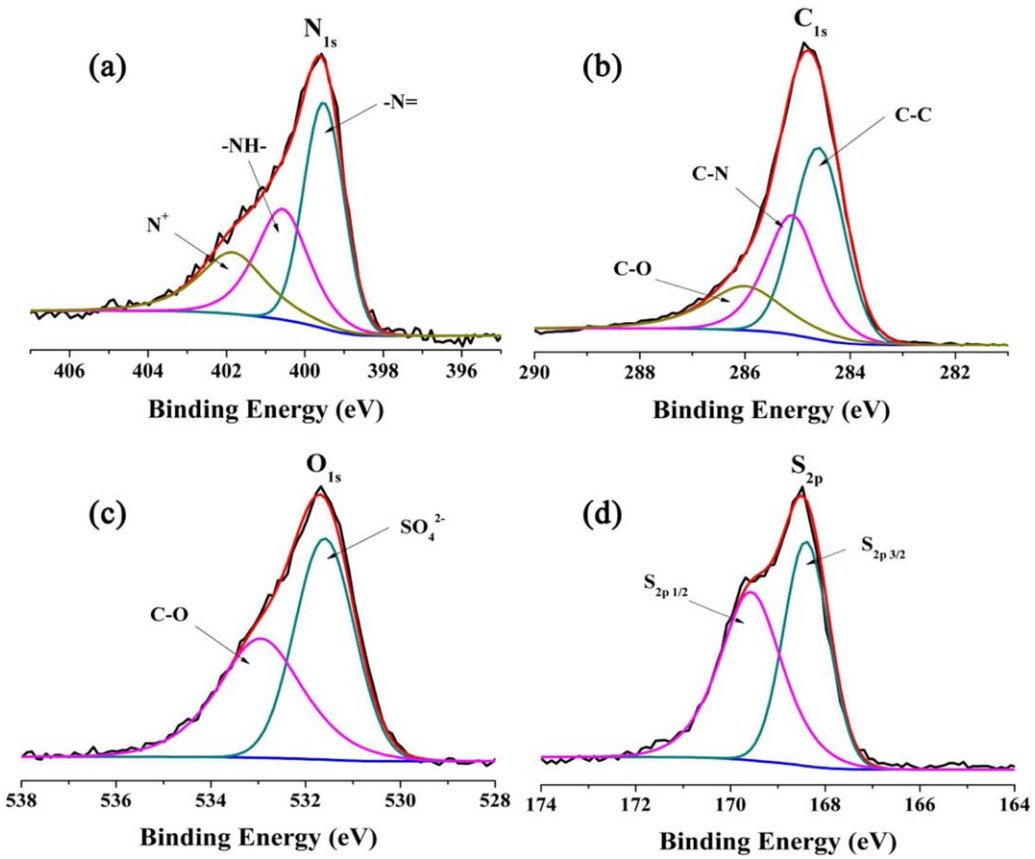

Figure 2. XPS spectra of (a) N1s, (b) C1s, (c) O1s, and (d) S2p signals for PANI at a PVA/ANI ratio w/w of 0.063. [Color figure can be viewed in the online issue, which is available at wileyonlinelibrary.com.]

vis spectra [Figure 4(b)]. In contrast to the literature,[5,12,30,43,60] the peak boundaries in the UV–vis spectra, represented by π–π^* transition (340–360 nm) and polaron band π–π^* transition (440–460 nm), were indistinct and connected nearly into one peak under a low PVA/ANI ratio. This pointed to the intermediate state between the π band and polaron π band reducing the required band energy and resulted in the high conductivity of this type of PANI. In comparison to other literatures,[43,61,62] the redshift of the broad peak around 800–890 nm was attributed to the π of the delocalized polaron band transition and implied the monopolaron form rather than the dipolaron or multipolaron form[63]; this also contributed to the high conductivity of PANI/PVA. However, the peaks at 340–360 nm turned into an individual peak at higher PVA/ANI ratios. Meanwhile, the peaks at 800–890 nm moved to lower wavelengths; this represented a higher transition energy, made the π to the delocalized polaron band transition difficult, and ultimately led to a lower conductivity. The absorption strength increased along with increasing PVA/ANI ratio; this corroborated with the dispersibility of PANI/PVA in water. In addition, the presence of peaks at 440–460 and 800–

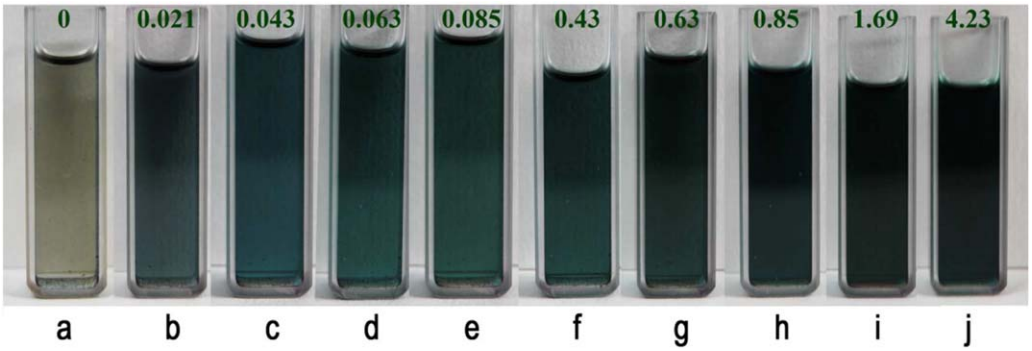

Figure 3. Digital image of the supernatant of PANI/PVA (1 mg) at different PVA/ANI ratios w/w sonicated in deionized water (10 mL) for 24 h. [Color figure can be viewed in the online issue, which is available at wileyonlinelibrary.com.]

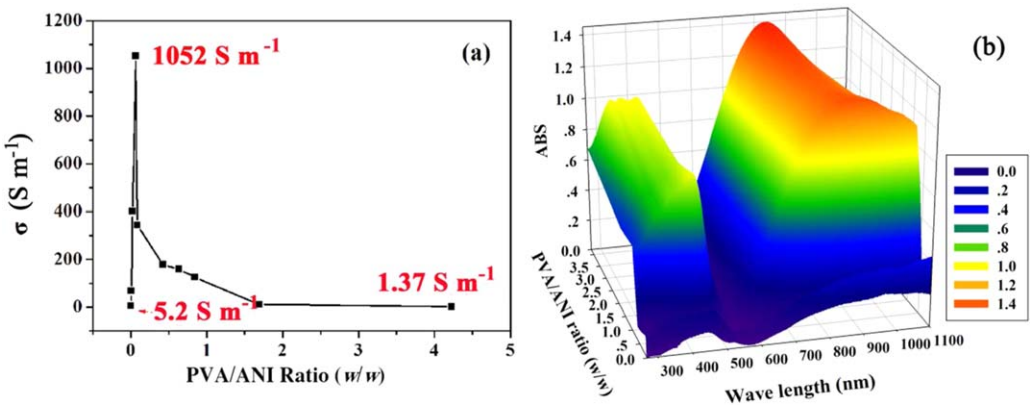

Figure 4. (a) Room-temperature conductivity (σ) of PANI as a function of the PVA/ANI ratio w/w. (b) UV–vis spectra (in water, *ABS* absorbance.) of PANI prepared with different PVA/ANI ratios. [Color figure can be viewed in the online issue, which is available at wileyonlinelibrary.com.]

890 nm with a high optical absorbance brought about dark green coloring for the PANI composites; this is also an important characteristic property of conducting PANI (Figure 3).

2. Second, PVA as a polymer solution enabled the charge carrier both move along and between chains. PVA chains played the role of a bridge in the process of charge-carrier transfer and made the charge carrier move along polymer chain and hop the interchain more easily.
3. Third, the changes in the density and mobility of the charge carriers were possibly associated with the particular structure of PANI imprinted from PVA formed in the aqueous solution. As a result, the additive PVA promoted the conductivity of PANI.

Even so, the conductivity dropped with the further increasing PVA/ANI ratio beyond a maximum value. As mentioned previously, the PVA chains incorporated with PANI by hydrogen bonds; this led the PVA not being easy to remove in the purification steps. An excess of nonconducting impurities was present between the polyaniline chains and endowed the PANI with excellent dispersibility or solvability in the solvent (Figure 3), but at the same time, it hindered the interchain charge-carrier transition. When the interchain charge mobility dropped further, this resulted in a reduction in the conductivity.

As is well known, when PANI was in a perfect EB form, 50% oxidized with alternative quinoid and benzenoid rings, and 50% doping resulted in the protonation of the entire quinoid ring; this led to the formation of perfect polarity and a high achievable conductivity.[31] That is, the conductivity improved further along with increasing doping level.

Electrochemical Performance

To further estimate the performance of the composite as electrode material for supercapacitors, the plate electrode was fabricated. Figure 5(a) shows the specific capacity of the PANI composite electrode, as calculated from their galvanostatic charge/discharge curves tested in a 1*M* H_2SO_4 aqueous solution at a current density of 0.5 A/g within a potential window of −0.2 to 0.8 V versus SCE. The curves exhibited an increase followed by a decrease along with the magnification of the PVA/ANI ratio. The discharge-specific capacitance of the PANI composite was as high as 382.9 F/g at a current density of 0.5 A/g (PVA/ANI ratio = 0.21 w/w). Figure 5(b) shows the galvanostatic charge/discharge curves of PANI/PVA (PVA/ANI ratio = 0.21 w/w) tested at different current densities. The calculated specific capacitances were 314 F/g at 1 A/g and 235 F/g at 2 A/g, respectively.

The high-power characteristic is one of the basic requirements for an electrode material in supercapacitors, which can be identified from their voltammetric response at various scan rates. This property of the PANI composite is shown in Figure 5(c,d). The CV curves [Figure 5(c)] showed two redox couples, that is, peak 1/peak 3 (P1/P3) (0.22/0.10 V) and peak 2/peak 4 (P2/P4) (0.46/0.44 V). The redox transitions at lower positive potentials corresponded to the well-known transition of PANI from its semiconducting state (leucoemeraldine) to the conductive form (emeraldine), whereas the ones occurring at higher positive potentials corresponded to the overoxidation of the polymer followed by hydrolysis to a quinone-type species (pernigraniline). Apparently, each curve exhibited a similar shape, but the total current increased with increasing scan rates. Even at a scan rate of 100 mV/s, the CV curve still appeared in two pairs of redox peaks; this was indicative of a highly capacitive nature with a good ion response. The cathodic peaks shifted positively, and the anodic peaks shifted negatively with incremental changes in the potential scan rates from 10 to 100 mV/s. The peak potential shifted less than 30 mV per 10-fold change in the scan rate; this indicated that the PANI composite was beneficial to fast redox reactions, good ion response, and a short diffusion path of electronic transport. A plot of the current density at the oxidation peak around 0.22 V versus the subduplicate scan rate is given in Figure 5(d). The near linear dependence of the current density on the subduplicate scan rate associated with the diffusion control mechanism further revealed good reversible stability and a fast response to oxidation/reduction with current changes. These results demonstrate a high-powered delivery or uptake of the PANI composite electrode material.

The Nyquist plot was used to study the redox processes of the PANI composite and to evaluate their ionic and electronic conductivity and specific capacitance. A typical Nyquist plot of a

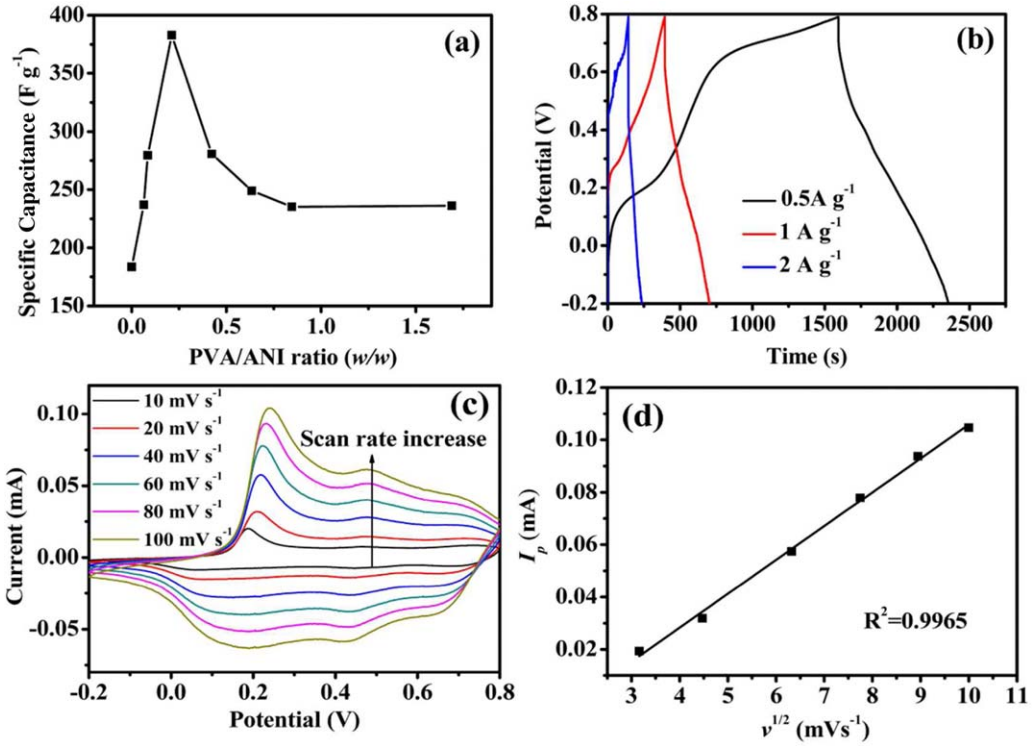

Figure 5. (a) Specific capacity of PANI/PVA with different PVA/ANI ratios calculated from galvanostatic charge–discharge curves at a current density of 0.5 A/g. (b) Charge–discharge curves tested at different current densities in a 1*M* H_2SO_4 aqueous solution within a potential window of −0.2 and 0.8 V versus SCE. (c) CV curves at different scan rates from 10 to 100 mV/s. (d) Subduplicate scan rate ($v^{1/2}$) versus the peak current of P1 (I_p) in the CV curves (Here R^2 is correlation coefficient.) For panels b–d, the PVA/ANI ratio was 0.021. [Color figure can be viewed in the online issue, which is available at wileyonlinelibrary.com.]

PANI composite electrode tested in a 1*M* H_2SO_4 aqueous is shown in Figure 6. Because the *x* axis of the Nyquist plot was the real component of impedance, a higher series resistance resulted in a shift to the right. The impedance plot could be divided into high-frequency and low-frequency components of the plot. A semicircle was observed in some of the composite electrodes in the high-frequency region; this was indicative of the charge-transfer phenomena of a Faradic process. The semicircle at the high frequency was nearly not detected for large proportions of electrodes; this suggested that the interfacial charge-transfer resistance was significantly low or the body impedance was too large. In the intermediate frequency region, the 45° line was characteristic of Warburg diffusion and was attributable to the semi-infinite diffusion of ions into the porous structure of the PANI composite electrode–electrolyte interface. The larger Warburg resistance indicated greater variations in the ion diffusion path lengths and increased the obstruction of ion movement. The reduced resistance of the composite may have been due in part to the network of the composite structure, which facilitated the efficient access of electrolyte ions to the PANI surface and shortened the ion diffusion path. In addition, it suggested that this part of the composites showed better capacitance than others. In the low-frequency region, there was a line almost vertical to the real axis in the imaginary part of the impedance; that is, this ideal capacitive behavior was due to the Faradic pseudo-capacitance of the composite electrode. The equivalent series resistance of the materials was the intercept of the plot with the real impedance (Z'), including both the solution resistance and the direct-current resistance.

The impedance measurement showed that the PANI composite electrodes possessed a lower internal impedance and a shorter diffusion path of the ions in the electrolyte. The introduction of the surfactant produced lots of networks; this was helpful for

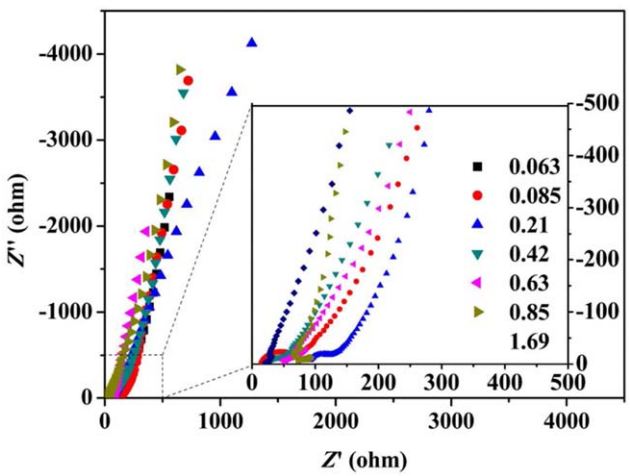

Figure 6. Nyquist plot of PANI/PVA synthesized with different PVA/ANI ratios (Here Z′ and Z″ are real and imaginary parts of impedance, respectively.) [Color figure can be viewed in the online issue, which is available at wileyonlinelibrary.com.]

reducing the internal resistance and increasing the electron transfer and electrolyte ion transport rate in the diffusion layer and benefited the enhancement of capacitance and the energy density of the PANI composite electrode.

CONCLUSIONS

In this study, a facile method was demonstrated to synthesize water-dispersible PANI with predominate conductivity. It was obvious that the additive PVA played an active role in promoting the conductivity to some extent. The conductivity of the PANI composite synthesized by this method was up to 1052 S/m; this was in the range of good semiconductors. It was promoted by two orders of magnitude compared to that of the original PANI and proved that if the synthetic methods were ameliorated, it could be further improved. Combined with the dissolved PVA through abundant hydrogen bonds, PANI/PVA possessed dispersible properties in aqueous solution, whereas when it was synthesized under a high PVA/ANI ratio, the composite was rigid and hardly porphyrized. The diffusion control mechanism revealed the good reversible stability and fast response to oxidation/reduction with the current changes for the PANI composite and ensured a high-powered delivery or uptake of the PANI composite electrode material. The specific capacitance value of the PANI composite synthesized by this method was also considerable under appropriate conditions. The introduction of PVA enhanced the capacitance and energy density of the PANI composite electrode. Moreover, the lower defect density and higher conductivity of the composite may have made a contribution to the higher capacitance and better rate capability.

ACKNOWLEDGMENTS

This article is dedicated to the memory of Professor Yanfeng Li.

This work was supported by the State Key Laboratory of Electrical Insulation and Power Equipment (contract grant number EIPE14304). The authors also gratefully acknowledge the financial support of the National Natural Science Foundation of China (contract grant number 51407140), the Fundamental Research Funds for the Central University (contract grant number XJJ2014023), the China Postdoctoral Science Foundation (contract grant number 2014M552448), and the Opening Foundation of the State Key Laboratory of Applied Organic Chemistry (contract grant number SKLAOC-2009-35).

REFERENCES

1. Zhang, D. C.; Zhang, X.; Chen, Y.; Yu, P.; Wang, H.; Ma, Y. W. *J. Power Source* **2011**, *196*, 5990.
2. Liu, C.; Li, F.; Ma, L. P.; Cheng, H. M. *Adv. Mater.* **2010**, *22*, E28.
3. Liu, T. Y.; Finn, L.; Yu, M. H.; Wang, H. Y.; Zhai, T.; Lu, X. H.; Tong, Y. X.; Li, Y. *Nano Lett.* **2014**, *14*, 2522.
4. Wang, Z. L.; He, X. J.; Ye, S. H.; Tong, Y. X.; Li, G. R. *ACS Appl. Mater. Interfaces* **2014**, *6*, 642.
5. Murthy, A.; Manthiram, A. *Chem. Commun.* **2011**, *47*, 6882.
6. Zhai, D. Y.; Liu, B.; Shi, Y.; Pan, L. J.; Wang, Y. Q.; Li, W. B.; Zhang, R.; Yu, G. H. *ACS Nano* **2013**, *7*, 3540.
7. Bu, Y. Y.; Chen, Z. Y. *ACS Appl. Mater. Interfaces* **2014**, *6*, 17598.
8. Xu, S.; Minteer, S. D. *ACS Catal.* **2014**, *4*, 2241.
9. Langer, J. J.; Mi1adowski, B.; Golczak, S.; Langer, K.; Stefaniak, P.; Adamczak, A.; Andrzejewska, M.; Sojka, L.; Kalisz, M. *J. Mater. Chem.* **2010**, *20*, 3859.
10. Bourdo, S. E.; Saini, V.; Piron, J.; Al-Brahim, I.; Boyer, C.; Rioux, J.; Bairi, V.; Biris, A. S.; Viswanathan, T. *ACS Appl. Mater. Interfaces* **2012**, *4*, 363.
11. Barman, T.; Pal, A. R. *ACS Appl. Mater. Interfaces* **2015**, *7*, 2166.
12. Kuila, B. K.; Stamm, M. *J. Mater. Chem.* **2010**, *20*, 6086.
13. Saini, P.; Choudhary, V. *Indian J. Pure Appl. Phys.* **2012**, *51*, 112.
14. Saini, P.; Choudhary, V.; Dhawan, S. K. *Polym. Adv. Technol.* **2012**, *23*, 343.
15. Saini, P.; Arora, M.; Gupta, G.; Gupta, B. K.; Singh, V. N.; Choudhary, V. *Nanoscale* **2013**, *5*, 4330.
16. Saini, P.; Choudhary, V.; Dhawan, S. K. *Polym. Adv. Technol* **2009**, *20*, 355.
17. Saini, P.; Choudhary, V. *J. Mater. Sci.* **2013**, *48*, 797.
18. Saini, P.; Choudhary, V.; Vijayan, N.; Kotnala, R. K. *J. Phys. Chem. C* **2012**, *116*, 13403.
19. Saini, P.; Choudhary, V. *J. Nanopart. Res.* **2013**, *15*, 1415.
20. Saini, P.; Arora, M. *J. Mater. Chem. A* **2013**, *1*, 8926.
21. Tian, Z. F.; Yu, H. J.; Wang, L.; Saleem, M.; Ren, F. J.; Ren, P. F.; Chen, Y. S.; Sun, R. L.; Sun, Y. B.; Huang, L. *RSC Adv.* **2014**, *4*, 28195.
22. MacDiarmid, A. G.; Epstein, A. *J. Faraday Disc. Chem. Soc.* **1989**, *88*, 317.
23. Li, G. R.; Feng, Z. P.; Zhong, J. H.; Wang, Z. L.; Tong, Y. X. *Macromolecules* **2010**, *43*, 2128.
24. Huang, J. X.; Moore, J. A.; Acquaye, J. H.; Kaner, R. B. *Macromolecules* **2005**, *38*, 317.
25. Long, Y. Z.; Chen, Z. J.; Zheng, P.; Wang, N. L. *J. Appl. Phys.* **2003**, *93*, 2962.
26. Li, G.; Jiang, L.; Peng, H. *Macromolecules* **2007**, *40*, 7890.
27. Chen, J. Z.; Li, B.; Zheng, J. F.; Zhao, J. H.; Jing, H. W.; Zhu, Z. P. *J. Phys. Chem. C* **2011**, *115*, 23198.
28. Sarnoa, D. M.; Manoharb, S. K.; MacDiarmida, A. G. *Synth. Met.* **2005**, *148*, 237.
29. Conklin, J. A.; Huang, S. C.; Huang, S. M.; Wen, T. L.; Kaner, R. B. *Macromolecules* **1995**, *28*, 6522.
30. Jafarzadeh, S.; Yhormann, E.; Ronnevall, T.; Adhikari, A.; Sundell, P. E.; Pan, J.; Claesson, P. M. *ACS Appl. Mater. Interfaces* **2011**, *3*, 1681.
31. Bhadra, S.; Khastgir, D.; Singha, N. K.; Hee Lee, J. *Prog. Polym. Sci.* **2009**, *34*, 783.
32. Nalwa, H. S. Handbook of Organic Conductive Molecules and Polymers; Wiley: Chichester, United Kingdom, **1997**.

33. Skotheim, T. A.; Elsenbaumer, R. L.; Reynolds, J. R. Handbook of Conducting Polymers; Marcel Dekker: New York, **1998**.
34. Ke, W. J.; Lin, G. H.; Hsu, C. P.; Chen, C. M.; Cheng, Y. S.; Jen, T. H.; Chen, S. A. *J. Mater. Chem.* **2011**, *21*, 13483.
35. Chaudhuri, D.; Kumar, A.; Rudra, I.; Sarma, D. D. *Adv. Mater.* **2001**, *13*, 1548.
36. Pomfret, S. J.; Adams, P. N.; Comfort, N. P.; Monkman, A. P. *Adv. Mater.* **1998**, *10*, 1351.
37. Luzny, W.; Banka, E. *Macromolecules* **2000**, *33*, 425.
38. Hong, E. Y.; Lee, S. H.; Lee, D. K.; Choi, S. S.; Baek, K. Y.; Hwang, S. S.; Kwon, O. P. *J. Mater. Chem.* **2012**, *22*, 18151.
39. Tarver, J.; Yoo, J. E.; Dennes, T. J.; Schwartz, J.; Loo, Y. L. *Chem. Mater.* **2009**, *21*, 280.
40. Lin, H. K.; Chen, S. A. *Macromolecules* **2000**, *33*, 8117.
41. Luo, J.; Zhang, H. M.; Wang, X. H.; Li, J.; Wang, F. *Macromolecules* **2007**, *40*, 8132.
42. Saini, P.; Jalan, R.; Dhawan, S. K. *J. Appl. Polym. Sci.* **2008**, *108*, 1437.
43. Bhadra, S.; Chattopadhyay, S.; Singha, N. K.; Khastgir, D. *J. Appl. Polym. Sci.* **2008**, *108*, 57.
44. Lin, Y. F.; Chen, C. H.; Xie, W. J.; Yang, S. H.; Jian, W. B. *ACS Nano* **2011**, *5*, 1541.
45. Xia, H. B.; Narayanan, J.; Cheng, D. M.; Xiao, C. Y.; Liu, X. Y.; Chan, H. S. O. *J. Phys. Chem. B* **2005**, *109*, 12677.
46. Zhou, C.; Han, J.; Guo, R. *Macromolecules* **2009**, *42*, 1252.
47. Stejskal, J.; Sapurina, I.; Trchova, M.; Konyushenko, E. N. *Macromolecules* **2008**, *41*, 3530.
48. Anilkumar, P.; Jayakannan, M. *Macromolecules* **2008**, *41*, 7706.
49. Meng, L.; Lu, Y.; Wang, X.; Zhang, J.; Duan, Y.; Li, C. *Macromolecules* **2007**, *40*, 2981.
50. Li, G. C.; Li, Y. M.; Li, Y.; Peng, H. R.; Chen, K. Z. *Macromolecules* **2011**, *44*, 9319.
51. Palaniappan, S.; John, A. *Prog. Polym. Sci.* **2008**, *33*, 732.
52. Laslau, C.; Zujovic, Z.; Travas-Sejdica, J. *Prog. Polym. Sci.* **2010**, *35*, 1403.
53. Surwade, S. P.; Agnihotra, S. R.; Dua, V.; Manohar, N.; Jain, S.; Ammu, S.; Manohar, S. K. *J. Am. Chem. Soc.* **2009**, *131*, 12528.
54. Tran, H. D.; Norris, I.; D'Arcy, J. M.; Tsang, H.; Wang, Y.; Mattes, B. R.; Kaner, R. B. *Macromolecules* **2008**, *41*, 7405.
55. Heeger, A. J.; Smith, P.; Cao, Y. *Macromol. Symp.* **1995**, *98*, 859.
56. Barbara, S. Infrared Spectroscopy: Fundamentals and Applications; Wiley: Weinheim, **2004**.
57. Pan, L. J.; Pu, L.; Shi, Y.; Sun, T.; Zhang, R.; Zheng, Y. D. *Adv. Funct. Mater.* **2006**, *16*, 1279.
58. Zhu, Y.; Hu, D.; Wan, M. X.; Jiang, L.; Wei, Y. *Adv. Mater.* **2007**, *19*, 2092.
59. Zhu, Y.; Ren, G. Q.; Wan, M. X.; Jiang, L. *Macromol. Chem. Phys.* **2009**, *210*, 2046.
60. Li, Y. Z.; Zhao, X.; Xu, Q.; Zhang, Q. H.; Chen, D. *J. Langmuir* **2011**, *27*, 6458.
61. Kan, J. Q.; Lv, R.; Zhang, S. L. *Synth. Met.* **2004**, *145*, 37.
62. Stejskal, J.; Sapurina, I.; Trchova, M. *Prog. Polym. Sci.* **2010**, *35*, 1420.
63. Huang, L. T.; Yen, H. J.; Liou, G. S. *Macromolecules* **2011**, *44*, 9595.